PERGAMON

International Journal of Solids and Structures 37 (2000) 1079–1097

INTERNATIONAL JOURNAL OF SOLIDS and STRUCTURES

www.elsevier.com/locate/ijsolstr

Predictive potentialities of a cylindrical structural cell for particulate elastomeric composites

V.V. Moshev*, L.L. Kozhevnikova

Institute of Continuous Media Mechanics, Russian Acadamy of Sciences, Academic Korolev Str. 1, 614013 Perm, Russia

Received 6 August 1998; in revised form 29 March 1999

Abstract

A unit cell of a specified shape under specified loading conditions has been offered for predicting some basic properties of particulate polymeric composites. The stress–strain state for bonded, debonding and debonded cells as a function of the cell stretch and superimposed pressure has been calculated for various filler volume fractions, adhesive strengths and matrix extensibility. The tensile curves and volume changes have been calculated for various superposed pressures. The predictive ability of the unit cell has been exemplified by the comparison of the calculated and experimental data on the modulus/filler volume fraction curves over a wide range of concentrations. © 1999 Elsevier Science Ltd. All rights reserved.

Keywords: Particulate composites; Structural cell

1. Introduction

The problem of searching representative volume elements in materials degrading under deformation has become an object of numerous publications in the last years. It is generally recognized that the microstructure damage events based on sound physical postulates help in explaining complicated macroscopic mechanical behavior of various materials. This situation is clearly in recent reviews of Murakami and Liu (1996) and Broberg (1997). The specificity of particular materials (polycrystalline metals and alloys, concrete, rock, polymeric composites) gives rise to a wide variety of approaches used. Most of papers are focused on such materials as polycrystalline metals and alloys, concrete, rock, and rigid composites.

Papers concerning polymeric particulate composites are scanty. Structural cells are often considered as some phenomenological objects (black boxes) whose behavior is derived mainly or partly from

* Corresponding author.

0020-7683/00/$ - see front matter
PII: S0020-7683(99)00110-9

Nomenclature

D	original diameter of the structural cell
L	original height of the structural cell
E_m	Young's modulus of the matrix
F	tension force of the cell
G and B	parameters in the equation for the elastic potential of the matrix material
P	pressure applied to the cell
R	radius of the spherical inclusion
S	surface of the inclusion opened by the matrix separation
U	elastic potential of the neo-Hookean matrix material
W	displacement of the top end of the cell relative to the bottom one
$\mathbf{C}$	Cauchy–Green deformation tensor
$\mathbf{g}$	unity tensor
$\mathbf{P}$	the second Piola–Kirchoff stress tensor
I_1 and I_3	the first and the third invariants of the Cauchy–Green deformation tensor
T_d	unit interface energy inclusion
U_c	elastic energy stored in the matrix volume of the cell
e_{ij}	component of the microstrain tensor within the matrix volume
e_1	maximum principal deformation in the matrix volume ($e_1=\lambda_1-1$)
e_b	breaking strain of the elastomeric matrix
s_{ij}	component of the true microstress within the matrix volume
s_0	mean stress in the matrix $s_0=(s_{11}+s_{22}+s_{33})/3$
λ_1	maximum microstretch within the matrix volume
$(s_0)_b$	dilation strength of the matrix
ε	deformation of the cell ($\varepsilon=W/L$)
ε_b	breaking strain of the cell
σ_{ij}	true stress component applied to the surface of the cell
φ	volume fraction of the inclusion in the cell, $\varphi=16/3(R/D)^3$
σ_z	mean normal stress applied to the end of the cell
η	ratio of the macroscopic Young's modulus of the cell to the Young's modulus of the matrix (relative modulus of the cell)

macroscopic behavior of appropriate materials (Anderson Vratsanos and Farris, 1993a, 1993b; Liu et al., 1998). Hence, the development of a cell as material unit, that contain sufficient information for predicting macroscopic behavior of a material and, at the same time, is based on physical concepts without enlisting macroscopic notions, may be regarded as a vital problem in today's material science.

Our efforts in the last few years have been focused exactly on this point, damageable particulate polymeric composites being the object of research (Kozhevnikova et al., 1993; Moshev and Kozhevnikova, 1996; Moshev and Kozhevnikova, 1997). In this approach, cells are considered as systems with a rather complicated internal substructure whose macroscopic behavior is deduced from the solution of appropriate boundary value problems. Such way of looking allows obtaining a large body of important information concerning structural damage, explains some features of macroscopic behavior of particulate composites and creates a more sound bridge in the field of the structure-properties gap. The satisfactory adequacy of the approach has been evidenced by comparing theoretical and experimental concentration curves for relative macroscopic modulus. However a number of points

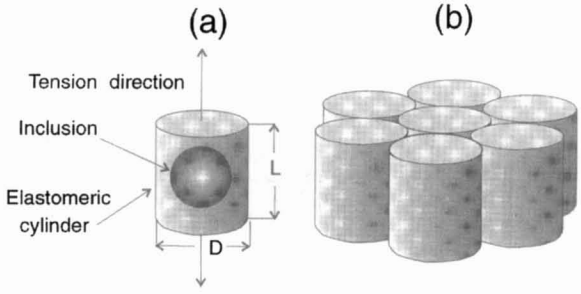

Fig. 1. Scheme of the structural cell (a) and its assumed packing (b).

remained to be studied in more detail to refine a model version suggested earlier by Moshev and Kozhevnikova (1997). In the present paper a closer attention is drawn to action of external pressure on the resistance and volume changes in structural cells.

2. Theoretical background

2.1. Model cell geometry, boundary and operating conditions

Cubic and cylindrical shapes are usual objects for examination. The papers by Andesson (1977) and Xia and Shih (1995) are recent examples of such approaches. In choosing the shape of the cell for the forthcoming research, we gave preference to the cylindrical one which is characterized by a remarkable feature that makes it more preferable. Having increased the radius of the spherical inclusion until it touches the lateral boundary of the cell, we come to the maximum filler volume fraction (inside the regularly packed cells) equal to 0.607 which is very close to that characterizing the ultimate packing of random structures composed of the uniformly-sized spheres (Bernal and Mason, 1960; Chong et al., 1971; Farris, 1968aFarris, 1968b). The maximum filler volume fraction in the compacted cubic cells cannot go beyond 0.525. We believed that the specificity of the cylindrical cell mentioned would provide better fit between the modeled and realistic behavior of particulate composites at high filler volume fraction.

With this in mind, a general scheme of the accepted structural cell shown in Fig. 1(a) represents an elastomeric cylinder (matrix), containing a solid spherical inclusion (filler particle) at the center. The height, L, of the cylinder equals its diameter, D. The cell is loaded by tension along the axis of the cylinder. It is supposed that, initially, the cell is well compacted with other cells of the same size [Fig. 1(b)] and continues to retain such state under tension. Meeting this requirement makes ends of the cell remain plane and its lateral surface keep cylindrical shape during extension.

In tension, a common mechanical evolution of the cell may be presented as it is shown in Fig. 2. Originally, the sphere is supposed to be perfectly bonded to the elastomeric matrix. During extension, this state is retained for some time [Fig. 2(a,b)]. However, when the intensity of the stress–strain state within the matrix reaches some limiting value, the cell looses the capability to keep its continuity. For highly elastic matrices, it is the detachment of the matrix from the sphere that most often takes place as a primary damage event [Fig. 2 (c)]. This postulate is based on the numerous experiments reported by Oberth and Bruenner (1965), Farris (1968a, 1968b), Struik et al. (1968), Sekhar and Van der Hoff (1971), Fedors and Landel (1975). The appearance of the transversal cracks inside the matrix phase is characteristic for poorly resilient non-rubber matrix materials. This point is discussed in more detail in Section 3.1.

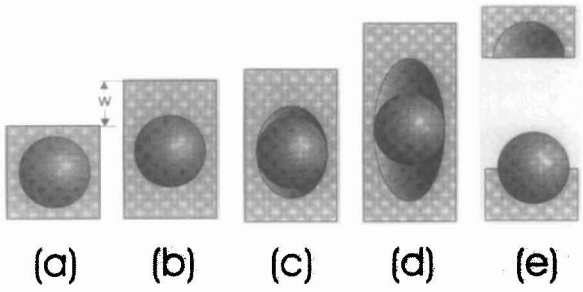

Fig. 2. Mechanical evolution of the cell in simple tension: (a) initial, (b) extended before separation, (c) the same after separation, (d) extended separated, (e) ruptured.

After the debond has occurred, an empty vacuole is formed above the pole zones of the sphere [Fig. 1(c)]. It is supposed that matrix separation proceeds from the both poles of the inclusion in a similar manner. However, the cell might not be regarded as failed after the debond has occurred. It continues to resist extension although with a significantly reduced rigidity [Fig. 2(d)] until secondary damage comes about. This one is the breakdown of the most strained matrix belt around the equator of the sphere [Fig. 2(e)]. The secondary damage means a final failure of the cell.

The resistance of the cell depends not only on its current stretch, but also on the value of the superimposed (external) pressure, especially after vacuole formation. Hence, in the analysis, the influence of both operating parameters (the cell extension and the superimposed pressure) on the stress–strain state of the cell and volume changes is to be taken into account.

Two crucial events in the outlined life-cycle of a structural cell most deeply affect its macroscopic behavior:

1. the matrix detachment from the inclusion, and
2. the matrix breakdown.

The first lowers the resistance of the cell, the second leads to its complete failure.

The analysis of the macroscopic behavior of cells concludes the paper.

2.2. Mechanical and ultimate properties of constituent materials

The approach adopted in this paper is purely elastic one. Only an equilibrium time-independent process is examined. The matrix phase is represented by a slightly compressible elastomer characterized by the elastic potential with two material parameters (Kozhevnikova et al., 1993)

$$U = \frac{G}{2}(I_1 - 3) + \frac{B}{8}(I_3 - 1)^2. \tag{1}$$

Here, the first item of the sum represents neo-Hookean elastic potential for incompressible material, where I_1 and I_3 are the first and the third invariants of the Cauchy–Green deformation tensor, **C**. G is a material constant, whose value is taken equal to 0.1 MPa, which corresponds to the shear modulus at small deformations or to the Young's modulus, 0.3 Mpa.

In recent publications of Blatz and Kakavas (1993), who experimented on elastomers, it was demonstrated that Poisson's ratio of realistic elastomers is about 0.49 due to small amounts of microscopic gas inclusions inevitably incorporated into rubber matrix during technological processing. For that reason, the second constant, B, corresponding to the bulk modulus of the rubber matrix at small deformations must be taken as equal to 5 Mpa.

The state equation derived from Eq. (1) has the form

$$\frac{1}{2}\mathbf{P} - \left(\mathbf{g} - I_3\mathbf{C}^{-1}\right)\frac{G}{2} + \frac{B}{4}(I_3 - 1)I_3\mathbf{C}^{-1},$$

where $\mathbf{P}$ is the second Piola–Kirchoff stress tensor, $\mathbf{g}$ is the unity tensor.

The solid sphere is taken to be perfectly rigid. Hence, all the energy of deformation of the cell is stored within the matrix volume.

Two strength criteria for elastomeric matrix are postulated:

1. breaking strain, e_b, in uniaxial extension as a measure of its extensibility causing transversal crack origination;
2. ultimate mean stress, $(s_0)_b$ as a measure of hydrostatic resistance of matrix under tensile stresses giving causing pore nucleation.

The value of e_b changes widely from 100 to 1000% for common rubbers, according their chemical specificity and network structure. The value of $(s_0)_b$ will be taken as equal to 5/6 of Young's modulus of the matrix, according to the long term investigations by Gent (1990).

The solid inclusion is taken to be non-destructive.

2.3. Damage characteristics for a structural cell

From many experimental works, the paper by Gent and Park (1984) being taken as a typical example, one may postulate three types of damage when considering the assumed specificity of cells:

1. matrix transversal cracking in the well-bonded systems with poorly extensible matrices;
2. matrix separation from filler particles with a vacuole-shaped pore formation;
3. rupture of the debonded cells.

It is supposed that transversal crack appearance in the matrix leads to an immediate failure of the cell. In contrast, when vacuole first appears, growing in the direction of tension, the cell keeps its integrity for some time until the extensibility of the matrix in the most strained equatorial part becomes exhausted. Clearly, a knowledge of the stress–strain state in the matrix volume is needed for making quantitative strength analysis.

Two sources provoking debond appearance may be thought of. The first postulates the existence of small precursor debonds on the surface of filler particles that are unavoidable in the actual industrial conditions. In such a case, a Griffith's approach may be used to describe this crack propagation as it has been done, for instance, by Kendall (1971) and Gent (1980). This 'virgin' debond starts spreading, when the energy stored in the matrix volume due to cell extension reaches the magnitude sufficient to create new interface surface. This condition is usually expressed as follows

$$\frac{\mathrm{d}U}{\mathrm{d}S} = T_d, \tag{2}$$

where $\mathrm{d}U$ is the elastic energy release of the system needed to create a debond surface increment $\mathrm{d}S$, T_d is the unit interface energy, determining the bond level between matrix and inclusion. Obviously, crack growth cannot start from the very beginning of the extension. Only, when Eq. (2) has been satisfied, will the debond begin to propagate.

It is still unknown how the energy of the adhesive debond depends on the relation between the interfacial normal and tangential stress. We assumed this material parameter to be a constant

magnitude, which may then be introduced into calculations describing the crack propagation. That may be fulfilled as follows.

The current strain energy of the cell, U, is controlled and depends both on the cell extension, $\varepsilon = W/D$, and the degree of debond characterized by the crack area, S.

$$U = f_1(\varepsilon, S). \tag{3}$$

Eq. (2) may now be rewritten as

$$T_d = \frac{\partial(f_1(\varepsilon, S))}{\partial S} = f_2(\varepsilon, S). \tag{4}$$

Taking T_d to be some characteristic interface property and its value to be constant during the entire process of the matrix separation from the inclusion, an opportunity opens for establishing a definite correlation between ε and S characteristic of the cell passing from a completely cohesive state to a completely decohesive one.

The force, F, of cell extension is also a definite function of both the current values of ε and S

$$F = f_3(\varepsilon, S). \tag{5}$$

Having obtained the relation between ε and S from Eq. (4), one can easily calculate the tensile curve, F vs. ε, characteristic of the cell undergoing matrix separation.

Next, the question arises concerning the selection of reasonable values of T_d. Evidently, the minimal value of T_d is zero, which means that the matrix is originally debonded from the sphere. The opposite case is when the bond strength is higher than the proper strength of the matrix. Another approach can be utilized here for establishing the origination of the debond in tension. Oberth and Bruenner (1965) showed that when the tensile hydrostatic stress at the pole zone of an inclusion reaches the Young's modulus value or so, small microscopic cavities within the binder phase appear in this locality and give rise to a withdrawal of the matrix from the inclusion. Then, the peeling takes place along the thin matrix layer on the inclusion surface as in the case of the adhesive debond, the process being controlled by the T_d value characteristic of the proper tear energy of the matrix material.

From this point of view, distinction between adhesive and cohesive debonding is of little concern. Thus, one may conclude that it is the tearing energy of elastomers that defines the upper limit of the bond strength. T_d in such cases, may be taken as being equal to the cohesive tearing energy of a corresponding elastomer.

According to Gent and Tobias (1982), the threshold tear strength of a hydrocarbon elastomer correlates with its Young's modulus. The use of this correlation has permitted us to specify the threshold tear strength for the matrix examined in this paper at the level of 150 J/m^2. This value might be regarded at the same time as the highest T_d magnitude characterizing cohesive matrix detachment and the highest tensile effort prior to the debond onset. It is clear that the adhesive debond energies must be of a lesser value.

2.4. Calculation procedure

The detailed description of the calculation method is published elsewhere (Kozhevnikova et al., 1993). For the solution of the boundary value problem, a functional of a special form is offered and used

$$He(H, \bar{\mathbf{u}}) = \int_{V_0} \left(AH(I_3 - 1) - A^2\left(\frac{\alpha}{2}\right)H^2 + W_1(I_1) + \frac{G}{4}((I_3 - 1) - A\alpha H)^2 - \rho^0 \bar{\mathbf{K}} \right) \mathrm{d}V_0 - \int_{S_p^0} \bar{\mathbf{p}}\bar{\mathbf{u}}\, \mathrm{d}S_p^0,$$

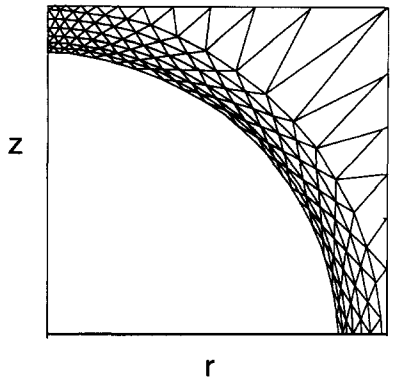

Fig. 3. Sketch of the finite element grid adopted for calculations for a filler volume fraction of 40%.

where $A=BG/(2(B-G))$ and $\alpha=4/B$; $\bar{\mathbf{u}}$ is the displacement vector; V_0 is the undeformed volume with volume forces, $\bar{\mathbf{K}}$, density, ρ^0, and the surface S_p^0, where forces, $\bar{\mathbf{p}}$, are applied; $AH=\sigma$ is the normalized quantity of σ.

The variations of this functional in H and $\bar{\mathbf{u}}$ leads to known variational equations of continuum mechanics for large deformations.

The finite element method was used for calculations. A typical sketch of the adopted finite element grid is shown in Fig. 3 for a filler volume fraction of 40%. Considering the geometry of the cell, a condensation of elements near the inclusion was performed.

Displacement vector components and the function H were approximated by the shape function Ψ_P and Φ_N. Then the displacements become $u_p = \Psi_n u_p^n$ and the function $H=\Phi_N H^N$, where u_p^n is the value of the vector component u_p in n-node, while H^N is the H value in N-node.

A program was developed for the incremental load procedure, using triangular cylindrical finite elements with a square approximation to the displacement field, and linear functions H. In contact zones, the conditions for non-penetration and non-positiveness of normal pressure, were introduced.

3. Microstress and microstrain distributions in the matrix phase of cells

It is obvious that the distribution of stresses and strains must depend strongly on the state of the cell. Hence it seems reasonable to examine separately bonded, debonding and debonded states of the cell.

The action of two parameters defining test conditions, i.e. the cell's extension, ε, and the external pressure, P, will be examined.

Remembering that the spherical inclusion as a constituent of the structural cell is taken to be perfectly rigid and non-destructive, the analysis of the internal state of the cell will cover only the examination of the stress–strain state of the matrix and the volume changes of the cell caused by the proper matrix compressibility and induced by vacuole appearance and evolution.

According to previous discussions, two representative quantities of the stress–strain state of the rubbery matrix are chosen for further analysis: the maximum principle strain, e_1, as an invariant characterizing the *intensity of deformation* and the mean stress, s_0, as a measure of *hydrostatic intensity of stress state*. In this paper, the value of e_1 is presented as $e_1=\lambda_1-1$, where λ_1 is the maximum principal stretch. The value of s_0 is the mean of three principal true stresses.

Most of the quantitative data to be presented in the subsequent analysis as illustrations have been obtained from calculations for a cell containing 30% by volume solid phase, extended to 10% and affected by zero and 0.1 MPa external pressures.

Figures will present the e_1 and s_0 distributions for imposed conditions as shadow patterns: the higher the level of the strain or stress, the lighter the shadow. Such patterns are to be regarded primarily as qualitative estimations for getting general orientation, although most important numerical data needed for analysis are indicated in critical localities.

3.1. Bonded cells

For a perfectly bonded cell, it may be safely suggested that the strain distribution in the matrix is determined basically by the degree of its extension since the influence caused by superimposed pressure cannot be significant due to minor compressibility of the rubbery matrix.

Fig. 4(a–d) presents e_1 and s_0 distributions at the test conditions mentioned above. Strain patterns (Fig. 4(a) for $P = 0$ and (b) for $P = 0.1$ MPa) are close to each other. It is seen that the most strained localities are situated above the poles of the sphere and along its surface at an angle of about 45° with respect to the z-axis direction. For 30% filler volume fraction, the maximum strains are 4–5 times

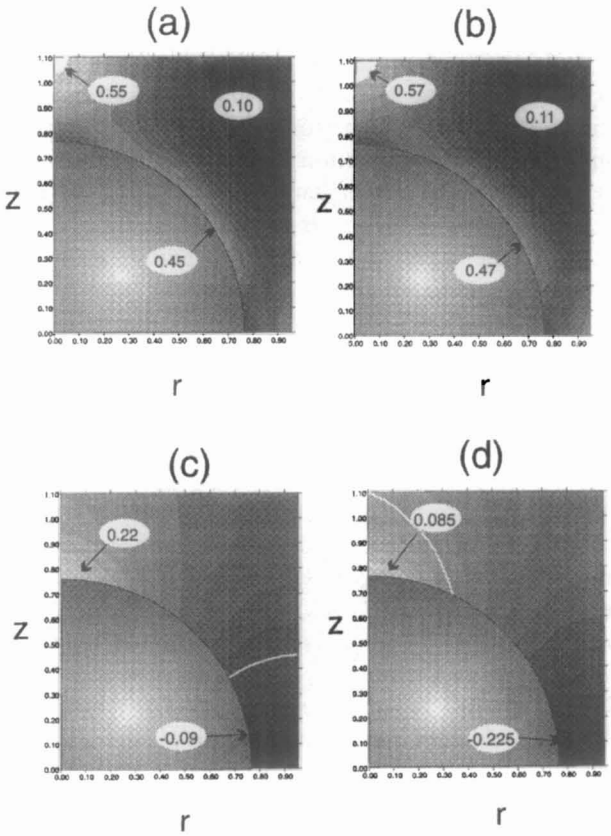

Fig. 4. e_1 (a, b) and s_0 (c, d) distributions at zero (a, c) and 0.1 MPa (b, d) superimposed pressure in a bonded cell. White lines in (c) and (d) demarcates the regions of positive and negative mean stresses.

greater than the proper strain of the cell. However, the polar maximum seems to be more critical than that adjacent to the sphere surface: it is somewhat greater and is positioned in a zone with higher hydrostatic tension than the near-wall one.

The s_0-distribution, in contrast to the e_1-distribution, is strongly responsive to the superimposed pressure (Fig. 4(c) for $P = 0$ and (d) for $P = 0.1$ MPa). In both cases, the volume of the matrix can be decomposed in two subdomains with positive and negative mean stresses, whose separation is shown as a white line in Fig. 4(c,d). A zone of the maximum hydrostatic extension (about 0.22 MPa) is localized at the pole of the inclusion [Fig. 4(c)], while that of the maximum hydrostatic compression (about −0.09 MPa) in Fig. 4(c) surrounds the equator of the inclusion. Pressurization of the cell increases the volume falling under the compressive mean stresses and diminishes strongly the maximum tensile mean stress at the pole from 0.22 to 0.085 MPa [Fig. 4(d)]. At higher pressures, the hydrostatic tension inside the matrix is eliminated completely.

Fig. 4 gives a clear general idea about the qualitative specificity of the strain and stress distributions and plausible sources and sites of damage appearance. Calculations show that, as to positioning of critical localities, this pattern remains the same for other solid volume loadings (Moshev and Kozhevnikova, 1997).

Inside the matrix, two sites of damage issuing from the stress–strain analysis may be inferred. The first is what one might call a *distortion* damage. It arises at the locality where e_1 reaches the breaking strain of the matrix, e_b, i.e. at the ends of the cell, and has a form of a transversal crack, as was demonstrated in the experiments of Gent and Park (1984) or Dekkers and Heikens (1985). The second is what one might call a *decohesion* damage. It arises in the matrix close to the pole of the inclusion as a tiny onion-shaped tear, when s_0 in this place reaches a magnitude approximately equal to the matrix modulus, E_m. Tear appearance triggers matrix separation with a crack propagating along the surface of the inclusion, the thin matrix level remaining intact on the solid surface (Gent and Park, 1984; Oberth and Bruenner, 1965).

Besides these two modes of damage, there exists the third one, that of pure interface debond, emerging when the energy of the adhesive tearing is less than that of the matrix. The interface failure gives rise to an appearance of a curvilinear crack similar to that from the matrix decohesion.

In the framework of the model in question, the appearance of the cross-cut crack, as a result of a poor extensibility of the matrix material, is regarded as a complete failure of the cell, while the decohesive and adhesive phenomena near the pole of the inclusion giving rise to the interface separation may be considered only as some primary pore-forming damage not leading to the immediate failure of the cell. The answer to the question, which of these modes of damage is to occur first, depends on the test conditions (cell's extension and superimposed pressure), matrix properties (Young's modulus and extensibility), adhesive debond energy, and filler volume fraction determining strain and stress concentrations.

It is clear that the case of perfect bond between the matrix and the filler benefits the transversal crack breaking mode to the utmost extent. This crack is to occur inside the matrix near the ends of the cell, where longitudinal straining of the matrix reaches maximum as it follows from Fig. 4(a,b). In this place, the strain of the matrix, e, is controlled mainly by the strain of the cell, ε, and the strain concentration factor, k_t, called forth by the filler volume fraction, φ. Hence, the value of e is found simply as a product of ε and k_t. The transversal crack appears when e reaches the breaking strain of the matrix material, e_b. This dependence is depicted in Fig. 5, where the breaking strain of the cell, caused by transversal cracking $(\varepsilon_b)_t$, is represented as a function of φ for various breaking strains of the matrix material, e_b.

At the same time, matrix decohesion, provoked by the cavitation near the pole of the sphere by the hydrostatic tension is determined by the strain of the cell, ε, hydrostatic stress concentration factor, k_h, (as a function of the filler volume fraction) and external pressure, P. The cavitation and the immediate

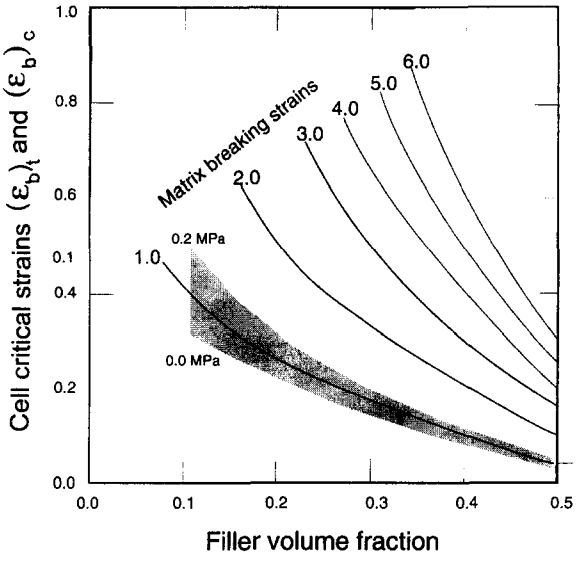

Fig. 5. $(\varepsilon_b)_t$ as a function of the filler volume fraction for different breaking strains of the matrix material (solid lines) and $(\varepsilon_b)_c$ as a function of the filler volume fraction and external pressure in he range between zero and 0.2 MPa (shadowed stripe).

matrix separation occur when the value of the hydrostatic tension (under imposed P) reaches the value of the Young's modulus of the matrix.

The correspondent critical strain of the cell, $(\varepsilon_b)_c$, as a function of filler volume fraction for the range of P from zero to 0.2 MPa, is also shown in Fig. 5 as a shadowed strip.

It follows immediately from Fig. 5 that, for all values of φ, cavitation, followed by matrix separation, always precedes transversal crack formations when the breaking strains of the matrix material are greater than 1.0; this is confirmed by experimental practice. Obviously, an adhesive debond, as a cause of the matrix separation, only favors this feature.

Corresponding empirical relations suitable for the range of φ from 0.1 to 0.5 are given below:

$$(\varepsilon_b)_t = \frac{e_b}{(1.83 - 12.39\varphi + 259.4\varphi^2 - 983.0\varphi^3 + 1313.6\varphi^4)},$$

$$(\varepsilon_b)_c = (0.416 - 1.19\varphi + 0.857\varphi^2)(1.0 + 0.363P - 0.0375P^2).$$

3.2. Debonding cells

A general estimation of the specificity of the strain and stress distributions in a partly debonded cell can be perceived from Fig. 6(a–d). This figure (similarly to Fig. 4) presents e_1 and s_0 distributions for the test conditions mentioned above. A drastic rearrangement of the strain and stress distributions, as compared with Fig. 4, takes place after matrix separation onset. A withdrawn, vault-like part of the matrix that previously exhibited the highest strains under tensile hydrostatic stresses, now experiences insignificant compression and is weakly strained. Maximum local straining shifts to the tip of the progressing curvilinear crack.

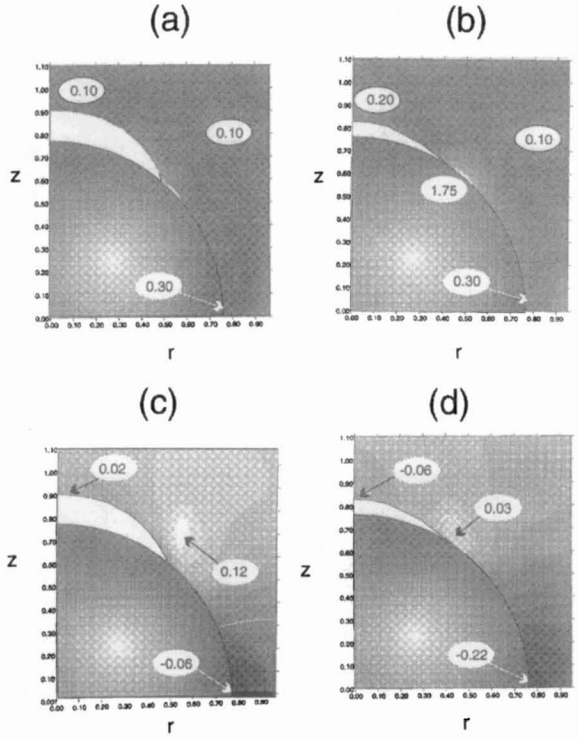

Fig. 6. e_1 (a, b) and s_0 (c, d) distributions at zero (a, c) and 0.1 MPa superimposed (b, d) pressure in debonding cell. White line in (c) demarcates the regions of positive and negative mean stresses. In (d), positive s_0 are concentrated around the tip of the crack.

Clearly, the finite element approach can provide only approximate estimations in this locality. Nevertheless, it gives some insight into the order of magnitude of the strains computed for the grid adopted. Calculated coefficients of the strain concentration are of the order of 30. This suggests that if the separation of the matrix has started, it will continue (led by the crack tip singularity) until the detachment is complete. During the crack propagation, other damage effects are hardly possible except for the moment when the crack tip approaches the equatorial zone. There, at the line of separation, the transversal cracks are sometime observed in experiments with matrices having moderate breaking strains.

Curiously enough, an application of external pressure to the cracked cell [Fig. 6(b)] leads to an augmentation of strains both in the dome and equatorial parts of the matrix; the high strains originate from the matrix dome flattening. Nevertheless, cracks are never observed experimentally in this zone, since the hydrostatic compression is possibly the strong impeding factor.

In the pressurized cell, the contact area between the matrix and the inclusion increases, and yet the point of the strain concentration remains at the tip of the closed crack [Fig. 6(b)].

Pressurizing diminishes the fraction of the matrix volume found under hydrostatic tension [Fig. 6(c,d)], reducing it to zero at high pressures. On the other hand, the extension of the pressurized cell always tends to increase the region of positive mean stresses and the result always represents a balance of these counteracting factors.

Calculations show that the general character of strain and stress patterns in cracked cells does not change basically with filler volume fraction.

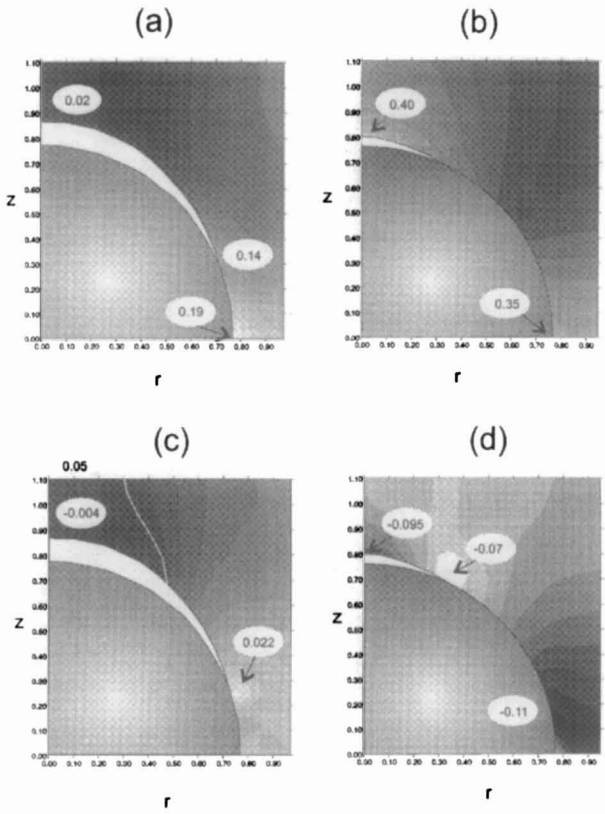

Fig. 7. e_1 (a, b) and s_0 (c, d) distributions at zero (a, c) and 0.1 MPa superimposed (b, d) pressure in debonded cell. White line in (c) demarcates the regions of positive and negative mean stresses. No positive s_0 exists in (d).

3.3. Debonded cells

After the crack propagation has reached the equatorial line, the cell may be judged as being fully debonded. A singular point disappears and, with it, the stress and strain concentrations. This is in a good agreement with the results of Dekkers and Heikens (1985) for a rigid sphere embedded into an infinite polymeric matrix. The strain magnification factor drops in the most strained equatorial matrix belt to an insignificant value of about 2, which depends weakly on the cell elongation.

Typical strain and stress distributions in completely debonded cells is exemplified in Fig. 7(a–d). The strain distributions [Fig. 7(a,b)] are similar to those observed in partly detached matrices [Fig. 6(a,b)]. Superposing pressure, again, drastically enhances the strains at the summit of the vacuole dome from 2% to about 50% [Fig. 7(c,d)]. At the equator, they are also raised but to a lesser extent (30%).

The high strain magnification above the pressurized vacuoles, called forth by the high transversal hydrostatic compression [Fig. 7(b)], as has been noted above, does not lead to crack formation. The stretched matrix belt in the equatorial part is also found to be under hydrostatic compression. These conditions impede crack origination and opening, and reinforce composites. The reinforcing action of pressurization is well corroborated in numerous experimental investigations (Farris, 1968a, 1968b; Oberth and Bruenner, 1965 and others).

The minimum hydrostatic compression [Fig. 7(d)] is localized along the line of matrix detachment. This fact and the vacuole presence might favor crack origination and opening. Perhaps this explains

why the matrix is commonly disrupted in this locality, rather than at the equator, where the strain is a trifle over that at the line of detachment. Taking into account the closeness of both magnitudes, a somewhat greater equatorial strain seems to be more suitable to use in the estimation of ultimate extensibility of the debonded cells by equalizing this strain to the breaking strain of the matrix material.

It has been found that the formula expressing this relationship is of the form

$$\varepsilon_b = \frac{e_b}{(1.8(1+190\varphi^{6.8})(1+0.58P^{0.45})},$$

where ε_b is the breaking strain of the cell, e_b is the breaking strain of the matrix material, φ is the filler volume fraction and P is the superimposed pressure.

4. Effective characteristics of cells

The foregoing analysis has been focused on the internal features of structural cells under extension. A transformation of *structural notions and relations*, used in solutions of boundary-value problems, into corresponding *macroscopic characteristics* of cells is the next step to continuum formulations.

For this, a substitution of the microstresses, s_{ij}, and microstrains, e_{ij}, that have been used, say, for inside-cell analysis, for macroscopic stresses, σ_{ij}, and strains, ε_{ij}, of a larger scale level, i.e. that of the cell characteristic size, is needed. This allows the cell to be presented as some uniform material unit. Based upon the assumed boundary conditions for cells, the normal nonuniform microstresses s_z and s_r at the ends and the lateral area of the cell (Fig. 8) may now be substituted for their averaged values σ_z and σ_r that may be regarded as common sense stresses on the boundary of a continualized material unit. In the following analysis, σ_z and σ_r will be presented as engineering values related to the initial cross-section of the cell model. The tensile strain of the cell, ε_z, is calculated simply as the ratio between the displacement of the ends, W, and the initial height of the cell, L. Hence, the notion of the macroscopic Young's modulus of the cell may be easily formulated as a ratio between σ_z and ε_z at $\sigma_r=0$.

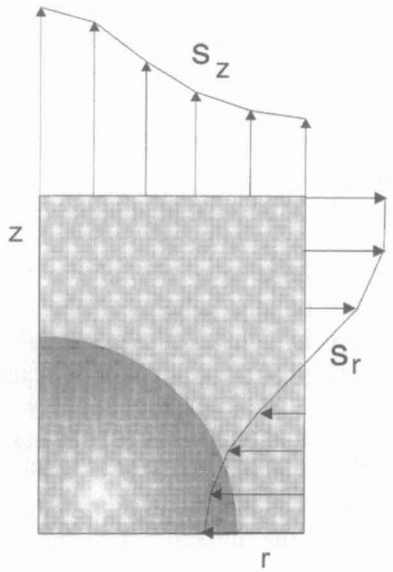

Fig. 8. Microstress distribution on the boundaries of the cell.

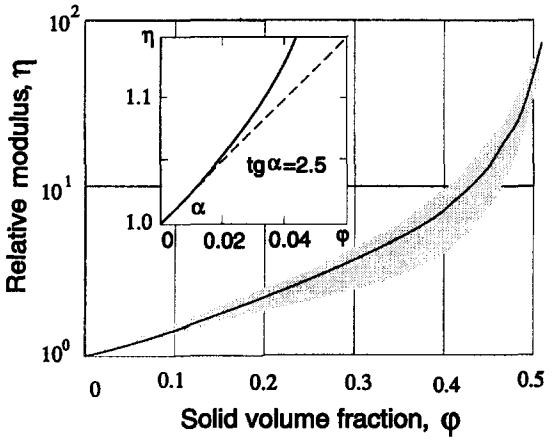

Fig. 9. Relative modulus vs. filler volume fraction for bonded cells: solid line is calculation, shadow is experimental.

The macroscopic behavior of the cell model will be represented by its stress–strain and volume–strain curves. A particular form of these relations is a function of many variables: φ, P, T_d, G, B, e_b and $(s_0)_b$. To exemplify the characteristic features of the macroscopic behavior of cells, a following set of the basic input data has been taken: $\varphi=0.3$, $P=0$, $T_d=100\ \mathrm{J/m^2}$, $G=0.1$ MPa, $B=5.0$ MPa, $e_b=2.0$ and $(s_0)_b=0.3$ MPa.

First, the predictive capability of the bonded cylindrical cell has been checked; the relative modulus was calculated as a function of filler volume fraction. Fig. 9 presents the obtained dependence in comparison with well-verified experimental data collected from various sources (shaded region) by Chong et al. (1971). The agreement between theoretical and experimental results may be judged as being good up to high concentrations. The theoretical curve lies somewhat higher than the averaged experimental data. Most likely, this is due to the fact that in actual systems, the directions of the cells are randomly inclined to the tension direction thereby decreasing the averaged resistance.

Of special interest is the initial part of the curve (up to 5% by volume) given as an inset in Fig. 9. The initial slope came out to be 2.5, which equals the well-known Einstein's coefficient in the formula for the viscosity of suspensions. This result not only testifies to a good predictive ability of the cell model, but also demonstrates that in specific cases, when one can neglect filler particle interactions, the macroscopic properties of a random system can be estimated from the analysis of properly characterized individual structural cells.

Tensile curves of cells are calculated according to the scheme of Fig. 2. First, the initial part of the curve with a slope characteristic of the bonded cell is calculated. Then the position of the point of separation on a σ–ε plot is established, as is indicated in Section 2.3 of this paper.

During the separation phase, the rigidity of the cell drops to a minimum, with a subsequent increase caused by the ever-continuing extension. The degree of rigidity drop depends on the filler volume fraction. At lower filler volume fraction (small sphere inside the assigned cell volume), the formation of the small vacuole can only slightly affect the resistance of the cell. By contrast, at higher filler volume fraction (large sphere inside the assigned cell volume), a large vacuole forms and the decrease in the cell's rigidity becomes considerable due to the marked narrowing of the equatorial matrix belt (Fig. 2). The cell breaks down when the strain of the fully debonded matrix at the equator reaches the breaking strain of the matrix material.

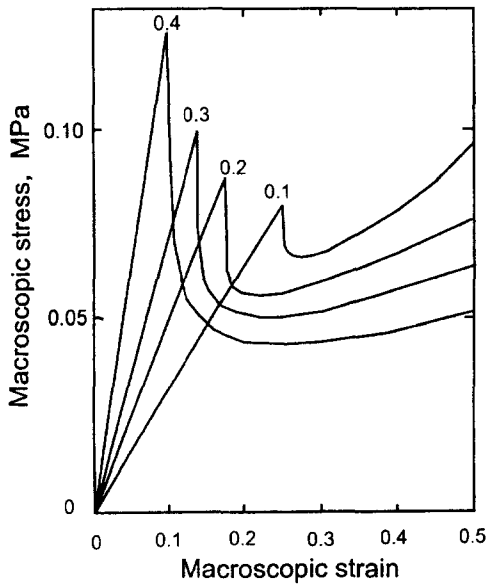

Fig. 10. Tensile curves at various filler volume fractions indicated near the curves for $P = 0.0$ and $T_d = 100\ J/m^2$.

Fig. 10 demonstrates how the shape of the tensile curves depends on the filler volume fraction. Increasing the filler volume fraction makes the drop of the cell rigidity deeper and the transition zone much wider.

The position of the transition curves strongly depends on the adhesive strength. The existence of small precursor cracks on the interface between the sphere and the matrix is postulated which trigger crack propagation according scheme given in Section 2.3. Nothing is known about the sizes and shapes of such initial imperfections. We assumed these cracks to be small enough not to markedly change the initial storing elastic energy of the cell, as compared with the perfectly bonded system.

Fig. 11 demonstrates the specificity of the adhesive energy influence. Lower T_d values entail lower

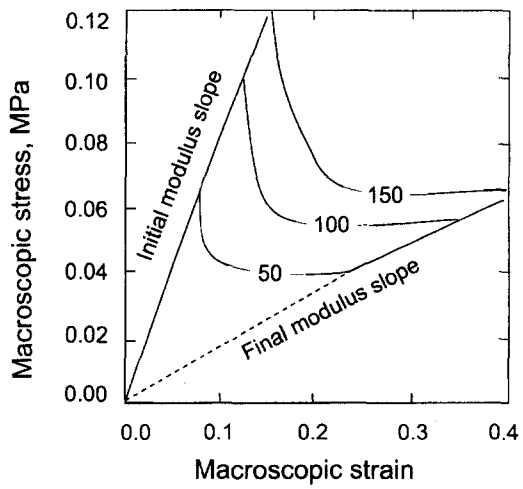

Fig. 11. Tensile curves at various interface bond energies T_d in J/m^2 indicated on the curves for $\varphi = 0.3$ and $P = 0$.

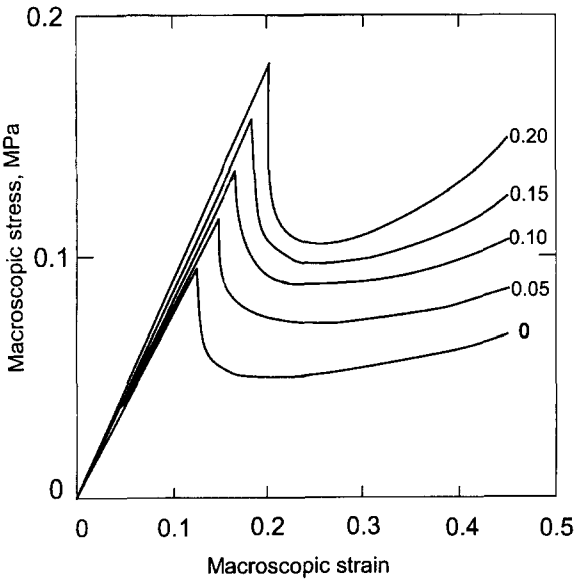

Fig. 12. Tensile curves at various superimposed pressures for $\varphi = 0.3$ and $T_d = 100\ \mathrm{J/m^2}$.

strains, at which the separation starts and, accordingly, the lower transition part of the tensile curve. The upper limit of the transition part is determined by the cohesive energy of the matrix, when the cavitation in the polar zone of the inclusion induces the separation process. In our case, it has been assumed to be $150\ \mathrm{J/m^2}$.

Fig. 12 depicts the influence of the superimposed pressure on the stress–strain behavior. It is seen that the resistance of the pressurized cell significantly increases due to the shrinking of the vacuole, accompanied with an increment in the elastic energy stored in the matrix. However, a gain in the rigidity increase with pressure slows down tending an asymptotic level corresponding to a complete vacuole closure.

Volume changes of the structural cell regarded as a continuum material unit are complicated. While the cell remains in the bonded state during the extension, the volume changes, with a good approximation, can be neglected. Then, after the separation has come about, a vacuole appears and grows. This state of the cell becomes highly responsive to the superimposed pressure. While the separation process is going on, the volume change is a function of the current stretch of the cell, the degree of separation and the superimposed pressure. The volume change during the extension of the initially bonded structural cell together with the correspondent tensile curves is shown in Fig. 13 for zero (a) and 0.1 MPa (b) external pressures.

After the separation has come to an end, the volume change becomes a function of two factors only: the current stretch of the cell and the superimposed pressure.

Fig. 14 demonstrates the influence of pressurization on the volume evolution of the debonded cell in extension. It is seen how the external pressure impedes the onset and magnitude of the volume growth.

5. Discussion of results

The data presented and examined above demonstrate that the offered structural cell (geometry, boundary conditions, mechanical properties of constituent elements) appears to be an efficient tool in

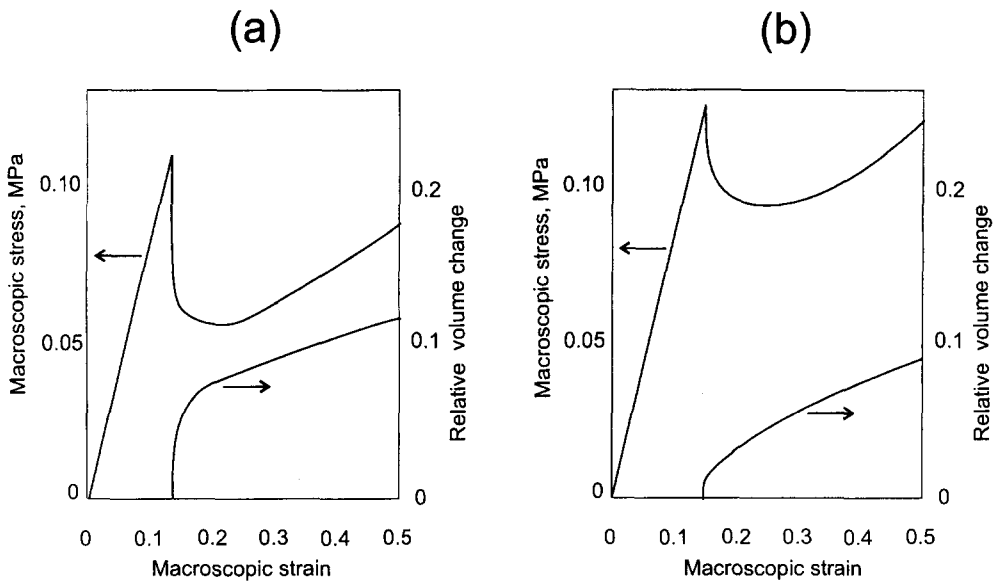

Fig. 13. Evolution of the tensile curves and the volume changes in extension under zero (a) and 0.1 MPa (b) superimposed pressure for $\varphi = 0.3$ and $T_d = 100\ \mathrm{J/m^2}$.

the elucidation of both microscopic and some macroscopic features of damageable particulate composites. The establishment of the macroscopic behavior of cells stemming from the solution of relevant boundary value problems seems to be a necessary condition for subsequent development of continuum constitutive relations based on structural ideas. The structural approach looks more representative than the usual phenomenology derived directly from experiments.

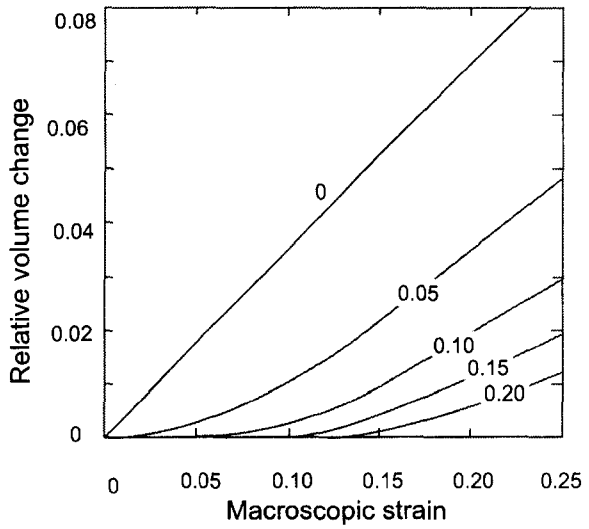

Fig. 14. Volume changes of the debonded cell in extension under various superimposed pressures values in MPa indicated on the curves for $\varphi = 0.3$ ($T_d = 0\ \mathrm{J/m^2}$).

Moreover, some important results can be obtained immediately from the examination of single cells. For instance, it is known that increasing external pressure does not lead to unbounded augmentation of the rigidity of composites: this process tends to flattening out with pressure. Usually, the plateau pressure and corresponding rigidity are found from experiments. Using structural cells allows one to directly predict the value of the maximum rigidity of cells caused by pressurizing, in relation to the filler volume fraction, the cell's elongation and rubber matrix modulus. In a like manner, the breaking strains of composites can be predicted as a first approximation. The evaluation of other macroscopic properties of the cells, for instance the compressibility, appears to be a good reference point in *a priori* estimations of the properties of composite systems. Such predictions are a great support for material scientists in designing new composite materials.

The cylindrical structural cell need further refinement focused on accounting for the visco-elastic nature of many polymeric matrices, the appearance of the interface sliding friction between the separated matrix and particles, and the time dependence of the cohesive and adhesive damages. Nevertheless, the knowledge already gained opens the way for attempts to construct a continuum description based exclusively on an available microstructural base.

6. Conclusions

A unit cell of a specified shape under specified loading conditions has been offered for predicting some basic properties of damageable particulate polymeric composites.

A method for the evaluation of the stress–strain state of cells under extension has been proposed and a variety of the boundary-value problems in the framework of large deformations has been solved.

Three sources of internal microdamage leading to a failure of the cell have been postulated: extreme local stretch and extreme local hydrostatic tension of the matrix constituents, as well as adhesive detachment of the matrix from the inclusion. A stress–strain analysis of cells has been carried out taking these damage events into account.

The macroscopic behavior of the structural cells reflecting bonded and debonded states has been established and the pertinent tensile curves, including the cell's breakdown, have been calculated. The influence of the filler volume concentration, adhesive bonding, external pressure on the tensile curves and volume changes has been demonstrated.

The good predictive ability of the approach has been exemplified by the comparison of the calculated and experimental data on the modulus/filler volume fraction curves over a wide range of concentrations.

References

Andesson, H., 1977. Analysis of a model for void growth and coalescence ahead of a moving crack tip. J. Mech. Phys. Solids. 25, 217–233.

Anderson Vratsanos, L., Farris, R.J., 1993a. A predictive model for the mechanical behavior of particulate composites. Part I: Model derivation. Polym. Eng. Sci. 33, 1458–1465.

Anderson Vratsanos, L., Farris, R.J., 1993b. A predictive model for the mechanical behavior of particulate composites. Part II: Comparison of model predictions to literature data. Polym. Eng. Sci. 33, 1466–1474.

Bernal, J.D., Mason, G., 1960. Computation of dense random packing of hard spheres. Nature 4754, 910–911.

Blatz, P.J., Kakavas, P., 1993. A geometric determination of void production in an elastic pancake. J. Appl. Polym. Sci. 49, 2197–2205.

Broberg, K.B., 1997. The cell model of materials. Computational Mechanics 19, 447–452.

Chong, J.S., Christiansen, E.B., Baer, A.D., 1971. Rheology of concentrated suspensions. J. Appl. Polym. Sci. 15, 2007–2021.

Dekkers, M.E., Heikens, D., 1985. Stress analysis near the tip of a curvilinear interfacial crack between a rigid spherical inclusion and a polymer matrix. J. Mater. Sci. 20, 3865–3872.

Farris, R.J., 1968a. Prediction of the viscosity of multimodal suspensions from unimodal viscosity data. Trans. Soc. Rheol. 12, 281–301.

Farris, R.J., 1968b. The influence of vacuole formation on the response and failure of filled elastomers. Trans. Soc. Rheol. 12, 315–334.

Fedors, R.F., Landel, R.F., 1975. Mechanical behavior of SBR–glass bead composites. J. Pol. Sci. Phys. Ed. 13, 579–597.

Gent, A.N., 1980. Detachment of an elastic matrix from a rigid spherical inclusion. J. Mater. Sci. 15, 2884–2888.

Gent, A.N., Tobias, R.H., 1982. Threshold tear strength of elastomers. J. Polym. Sci.: Polym. Phys. Ed. 20, 2051–2058.

Gent, A.N., Park, B., 1984. Failure process in elastomers at/or near a rigid spherical inclusion. J. Mater. Sci. 19, 1947–1956.

Gent, A.N., 1990. Cavitation in rubber: a cautionary tale. Rub. Chem. Techn. 63, G49–G52.

Kendall, K., 1971. The adhesion and surface energy of elastic solids. J. Phys. D: Appl. Phys. 4, 1186–1195.

Kozhevnikova, L.L., Moshev, V.V., Rogovoy, A.A., 1993. A continuum model for finite void growth around spherical inclusion. Int. J. Solids Structures 30, 237–248.

Liu, Y., Kageyama, Y., Murakami, S., 1998. Creep fracture modeling by use of continuum damage variable based on Voronoi simulation of grain boundary cavity. Int. J. Mech. Sci. 40, 147–158.

Murakami, S., Liu, Y., 1996. Local approach of fracture based on continuum damage mechanics and the related problems. Material Science Research International 2, 131–142.

Moshev, V.V., Kozhevnikova, L.L., 1996. Pressure reinforcement of particulate polymeric composites originated by adhesive debonding. J. Adhesion 55, 197–207.

Moshev, V.V., Kozhevnikova, L.L., 1997. Highly predictive structural cell for particulate polymeric composites. J. Adhesion 62, 169–186.

Oberth, A.E., Bruenner, R.S., 1965. Tear phenomena around solid inclusions in castable elastomers. Trans. Soc. Rheology 9, 165–185.

Sekhar, N., Van der Hoff, B.M.E., 1971. Cavity formation on elongation in filled elastomers. J. Appl. Pol. Sci. 15, 169–182.

Struik, L.C.E., Bree, H.W., Swarzl, F.R., 1968. Mechanical properties of highly filled elastomers. In: McClaren, M.L. (Ed.), Proc. Intern. Rubber Conf., 1967, pp. 205–231.

Xia, L., Shih, C.F., 1995. Ductile crack growth — II. Void nucleation and geometry effects on macroscopic fracture behavior. J. Mech. Phys. Solids 43, 1953–1981.